International Journal of Thermal Sciences 142 (2019) 266–279

Contents lists available at ScienceDirect

International Journal of Thermal Sciences

journal homepage: www.elsevier.com/locate/ijts

The effects of packing structure on the effective thermal conductivity of granular media: A grain scale investigation

Weijing Dai[a], Dorian Hanaor[b], Yixiang Gan[a,*]

[a] School of Civil Engineering, The University of Sydney, NSW, 2008, Australia
[b] Fachgebiet Keramische Werkstoffe, Technische Universität Berlin, Germany

ARTICLE INFO

Keywords:
Granular media
Packing structure
Grain-scale
Effective thermal conductivity
Discrete element method

ABSTRACT

Structural characteristics are considered to be the dominant factors in determining the effective properties of granular media, particularly in the scope of transport phenomena. Enhancing heat management requires an improved fundamental understanding of thermal transport in granular media. In this study, the effects of packing structure on heat transfer in granular media are evaluated at macro- and grain-scales. At the grain-scale, a gas-solid coupling heat transfer model is adapted into a discrete-element-method to simulate this transport phenomenon. The numerical framework is validated by experimental data obtained using a plane source technique, and the Smoluchowski effect of the gas phase is found to be captured by this extension. By considering packings of spherical SiO_2 grains with an interstitial helium phase, vibration induced ordering in granular media is studied, using the simulation method developed here, to investigate how disorder-to-order transitions of packing structure enhance effective thermal conductivity. Grain-scale thermal transport is shown to be influenced by the local neighbourhood configuration of individual grains. The formation of an ordered packing structure enhances both global and local thermal transport. This study provides a structure-based approach to explain transport phenomena, which can be applied in properties modification for granular media.

1. Introduction

Effective thermal management and waste heat dissipation are keys to improving efficiency in diverse industrial applications [1–3]. Towards this end, granular media are extensively used and are often studied by researchers in disciplines of thermal science and engineering [4–6]. Understanding and managing heat transfer processes in granular media necessitate the accurate evaluation of their effective thermal conductivity. Granular media can be generally regarded as multi-phase substances of which the effective thermal conductivity can be described by the Hashin-Shtrikman bound, Maxwell's equation and the effective medium theory [7,8]. However, these methods do not provide sufficient mechanistic insights, motivating further fundamental studies into thermal transport through granular media. Moreover, in a broader context, thermal transport has much in common with analogous phenomena of mass transfer and electrical conduction, thus, an improved understanding of heat transfer may serve to foment new insights these related fields.

For general binary solid-gas or solid-fluid granular media, major heat transfer pathways include: (1) heat conduction through solid particles, (2) heat transfer through solid-solid interfaces, (3) heat transfer through gas/fluid films near particle surfaces, (4) heat radiation between solid surfaces in solid-gas cases and from solid surfaces into nearby liquids in solid-fluid cases in high temperature condition ($T > 450K$) (5) convective heat transfer between solid and mobile gas/fluid, (6) natural convection in solids and fluids of high Rayleigh number, (7) heat transfer by macroscopic fluid flow [9], and (8) granular convective heat transfer due to the motion of solids [10]. Analytically, representative geometry methods have been widely used [11,12], which combine contributions from these aforementioned heat pathways according to the corresponding artificial geometries. In biphasic systems, cylinders [11,12] and cubic [13] have been used to determine the relative contributions of each pathway. To account for the dissimilarity between the representative geometries and the meso-scale structure of granular media, including grain size distribution, contact areas, and porosity, adjustable parameters are frequently applied. But such parameters are generally too coarse or artificial to meaningfully describe granular packing structures. Rather than using representative geometries, unit cell methods that derive effective thermal conductivity by integrating grain-scale contact unit cells [14–19] which are commonly formed two adjacent grains have also been developed. One advantage of unit cell methods is that they can

* Corresponding author.
E-mail address: yixiang.gan@sydney.edu.au (Y. Gan).

https://doi.org/10.1016/j.ijthermalsci.2019.04.028
Received 10 September 2018; Received in revised form 23 April 2019; Accepted 23 April 2019
1290-0729/

Nomenclature

Geometrical parameters of contact units

r_i, r_j	Radius of grains
r_{ij}	Effective radius of grain-grain contacts
$r_{\min}$	Minimum radius
h	Separation distance
D_{ij}	Distance between two centroids
d	Indentation depth
r_{cont}	Contact radius
r_{iw}	Effective radius of grain-wall contacts
r_{eff}	Effective radius of cylindrical thermal resistors
χ	Ratio between r_{eff} and r_{min}
L_{f}	Feature length of interstitial space

Parameters used to determine gas thermal conductivity

k_{g}	Thermal conductivity
k_{B}	Boltzmann constant
Kn	Knudsen number
γ	Energy transfer coefficient of gas
m_{s}	Molar mass of solid
m_{r}	Molar mass ratio $m_{\text{s}}/m_{\text{g}}$

Parameters used to characterise heat conduction and packing structure of granular media

k_{eff}	Effective thermal conductivity
k_{s}	Thermal conductivity of solid grain
α	Thermal conductivity ratio $k_{\text{s}}/k_{\text{g}}$
H_{cont}	Contact heat conductance
R_{cont}	Contact thermal resistance
R_{total}	Total thermal resistance of units
$R_{cyl.\,i}$, $R_{cyl.\,j}$	Thermal resistance of cylindrical thermal resistors
$\boldsymbol{Q}_{density}$	Heat flow density vector

Parameters used in finite element simulation

r_{c}	Radius of grains
ΔT	Temperature difference
Q_{FEM}	Heat flow
Q_{BOB}	Heat flow calculated by Batchelor & O'Brien model

Parameters used in discrete element simulation

Q_{inflow}	Inflow heat of entire media
L_{axis}	Axial height
ΔT_{gap}	Apparent temperature gap
$A_{\text{cross-section}}$	Cross-sectional area
Q_i	Heat flow of individual contacts
Q_{flow}	Total heat flow of grains
$\Delta T_{\text{gradient}}$	Fitted temperature gradient
k_{g}'	k_{g} by the Smoluchowski effect
P_{g}	Gas pressure
d_{g}	Kinetic molecular diameter
T	Thermodynamic temperature
m_{g}	Molar mass of gas
φ	Packing fraction of granular media
V_{Voronoi}	Volume of Voronoi cells
S_6	Structural index
$\boldsymbol{x}_i$	Contact vector
$\boldsymbol{k}^*$	Thermal conductivity tensor of grains
$\Delta \boldsymbol{T}_{\text{gradient}}$	Temperature gradient vector
k_{zz}	zz component in $\boldsymbol{k}^*$
θ_z	Thermal conductivity anisotropy

combine grain-scale heat transfer mechanisms with appropriate abstractions of packing structures, such as coordination number and packing fraction [14,18], under the assumption of isotropic and statistically homogeneous media. However, similarly to representative geometry methods, it is difficult to define such correlations in irregular packing structures using those quantifiable parameters [20], which requires suitable averaging methods. With development of computational power, discrete element methods (DEM) become favourable to study realistic irregular packing structures [21–23] for heat transfer purpose. One solution is to generate realistic packing structures to improve those abstractions of packing structures [24]. The other way is to directly simulate the heat transfer process by implementing the developed grain-scale thermal interactions [25–28], such as models in the unit cell methods [14,29–31].

Although well-established heat transfer models have been successfully adapted in DEM to describe granular media without overlooking the characteristics of packing structures [32–34], how to explain the effects of these characteristics is still unclear. By employing the grain-scale packing fraction as one of the variables [29] to derive heat transfer models, the importance of grain-scale packing structure is demonstrated. Nonetheless, effects of other structural characteristics remain inconclusive. It has been shown that the packing structure is of equivalent importance as packing fraction [35], but the question regarding the appropriate structural indicators to quantitatively characterise the effect of granular packings in heat transfer is as yet unanswered. Attempts have been made to investigate the influence of grain-scale stress network on thermal transport [36], but the link between such networks and granular packing structures requires further studies [37]. Relationships have been examined between effective mechanical properties and grain-scale order levels of packing structures [38,39]. Whether similar relationships can be established in the heat transfer context has not yet been discussed. The disorder-to-order transitions of granular media, in which crystallised and periodic packing structures are formed, have been recognised as one of the major events in agitated states [40] arising through shearing and vibration. It is therefore worth examining in depth the relationships between heat transfer and order of packing structures to further reflect the effects of external agitation on the effective thermal conductivity. Finally, it has been shown that pore-scale geometry is an influential factor in determining the permeability of composites [41], and the present work may be of further relevance towards mechanistic cross-scale analyses of percolation in porous media, as demonstrated in recent studies [42].

In the current study, the open source discrete element software LIGGGHTS [43] is modified to investigate packing and heat transfer in a generalised static solid-gas granular media. It is demonstrated that disorder-to-order transitions induced by vibration enhance the effective thermal conductivity of granular media as ordered packing structures lead to higher grain-scale thermal conductivity.

2. Grain-scale heat transfer model

In this work, contact units comprising two contacting or separated hemispheres are treated as individual grain-scale elements, and a modified Batchelor & O'Brien model is employed to describe intergranular heat transfer of these elements. Ideally, uniform temperature distribution within individual grains is assumed in the original Batchelor & O'Brien model [14], but this assumption introduces overestimation of heat transfer. To overcome this limitation, an equivalent temperature drop between the centroid and boundary of spheres is used

to account for the non-uniform temperature distribution [28,30,44]. This equivalent temperature drop usually depends on an empirical parameter based on matching specific experimental data. Here, we employed finite element analyses instead to acquire this essential model parameter numerically [28,30].

2.1. Basic solution

The original Batchelor-O'Brien (BOB) model considers granular media with large ratio α of solid thermal conductivity k_s to gas thermal conductivity k_g, i.e., $k_s/k_g \gg 1$ [14]. So, the temperature distribution within individual grains can be assumed constant. Two scenarios have been considered, a separated unit with separation distance h and a contacting unit with a circle contact surface of radius r_{cont}, as depicted in Fig. 1. Knowing the temperature difference ΔT between two centroids of one unit, the total heat flow Q_{BOB} across the unit has been analytically determined for both scenarios respectively [14]. Accordingly, the heat conductance H_{BOB} of the contact unit can be found by reducing ΔT, i.e., $H_{cont} = Q_{BOB}/\Delta T$.

When two grains are separated with $h \geq 0$, heat conductance H_{BOB} is expressed as

$$H_{cont} = \begin{cases} \pi\, k_g\, r_{ij} \ln \alpha^2 & \lambda < 0.01 \\ \pi\, k_g\, r_{ij} \ln\left[1 + \frac{r^{*2}}{r_{ij} h}\right] & \lambda > 100 \\ \text{Minimum value of the above two} & \text{else} \end{cases} \quad 2\text{-}1$$

In the above formulas, $\alpha = k_s/k_g$, $r_{ij} = 2\, r_i\, r_j/(r_i + r_j)$ and $\lambda = \alpha^2\, h/r_{ij}$. r^* is a numerical parameter used in the derivation of the BOB model, which is not exactly defined to certain values. Previous practices consider r^* related to an adjustable model parameter [30,44]. However, we defined r^* as r_{ij} in this work, because this enables us to determine an adjustable model parameter independent of the BOB model in latter sections. Although r^* has requirement of $r^* \gg \sqrt{r_{ij}\, h}$ according to the original derivation [14], common practices consider it as having negligible influence [30,44].

If two grains are in contact at a circular contact patch of radius r_{cont}, H_{cont} of this unit becomes

$$H_{cont} = \begin{cases} \pi\, k_g r_{ij} \left[\frac{2\beta}{\pi} - 2\ln\beta + \ln\alpha^2\right] & \text{if } \beta > 100 \\ \pi\, k_g r_{ij} \left[0.22\,\beta^2 - 0.05\ln\beta^2 + \ln\alpha^2\right] & \text{if } \beta < 1 \\ \text{Linear interpolation of the above two} & \text{else} \end{cases}, \quad 2\text{-}2$$

where $\beta = \alpha\, r_{cont}/r_{ij}$, positively related to the contribution by the contact patch relative to the total heat flow. r_{cont} is computed according to Hertzian contact mechanics by $r_{cont} = \sqrt{r_{ij}\, d/2}$, where d is the indentation depth. Further, d is defined as the difference between the sum of the radii of two contacting grains and the distance D_{ij} between two centroids of the corresponding grains, giving $d = (r_i + r_j) - D_{ij}$.

In addition, if a grain i forms a contact unit with a flat wall w, the wall can be approximated as a sphere of an infinitely large radius $r_w \to \infty$. In such case, r_{ij} is replaced by r_{iw} in the Eqns. (2)–(1) and Eqns. (2)–(2), where $r_{iw} = \lim_{r_w \to \infty} (2\, r_i\, r_w/(r_i + r_w)) = 2r_i$.

2.2. Inclusion of the Smoluchowski effect

The Smoluchowski effect relates to a reduced effectiveness of heat transfer through gases over scales comparable to the mean free path of gas molecules, as the result of boundary effects at solid-gas interfaces in granular media. This effect becomes significant in granular media, because gaseous phases in gaps between solids separated by short distances [45] in fact undertake the majority of transferred heat [14]. It brings about a dependence of gaseous heat transfer on gas pressure and grain size [18,28], and contributes to the deviation of α discussed in the previous section. To improve the BOB model, the Smoluchowski effect is implemented using the method described below, detailed in a previous work [28].

Fundamentally, the Smoluchowski effect is evaluated according to the molecular kinetic theory, using the ballistic heat transfer coefficient as the appropriate gas property. To differentiate this from the commonly used thermal conductivity, we refer to the equivalent thermal conductivity, described by

$$k_g' = \frac{k_g}{1 + 2\,\gamma\, Kn}, \quad 2\text{-}3$$

where γ quantifies the efficiency of energy transfer between gas molecules and the solid surfaces, and is given in terms of the molar mass ratio of the solid over gas by $m_r = m_s/m_g$,

$$\gamma = \frac{2\,(1 + m_r)^2 - 2.4\, m_r}{2.4\, m_r}, \quad 2\text{-}4$$

and the Knudsen number Kn is determined by the feature size L_f of a given space and the mean free path (MFP) of gas molecules as,

$$\mathrm{Kn} = \frac{MFP}{L_f} = \frac{k_B\, T}{\sqrt{2}\,\pi\, d_g^2\, P_g\, L_f}, \quad 2\text{-}5$$

where MFP is calculated by gas characteristics, including pressure P_g, thermodynamic temperature T, the kinetic molecular diameter d_g and the Boltzmann constant k_B. In the theoretical case of two parallel flat walls, L_f is the distance between two walls. But to determine k_g' in a contact unit, L_f is defined as the average distance between two corresponding grains [28]. The geometrical parameters of contact units of both the separated and contacting scenarios and brief mathematical procedure [28] used to obtain L_f are presented in Fig. 2, where r_{eff} is set as the minimum between r_i and r_j in each unit.

Following the method presented in Fig. 2, L_f of a pair of separated grains is calculated according to,

$$L_f = h + r_i\left(\frac{\sin^{-1}\left(\frac{r_{eff}}{r_i}\right) - \frac{r_{eff}}{r_i}}{\sin^{-1}\left(\frac{r_{eff}}{r_i}\right)}\right) + r_j\left(\frac{\sin^{-1}\left(\frac{r_{eff}}{r_j}\right) - \frac{r_{eff}}{r_j}}{\sin^{-1}\left(\frac{r_{eff}}{r_j}\right)}\right). \quad 2\text{-}6$$

In the contacting scenario,

$$L_f = r_i\left(\frac{\sin^{-1}\left(\frac{r_{eff}}{r_i}\right) - \sin^{-1}\left(\frac{r_{cont}}{r_i}\right) - \frac{r_{eff}}{r_i} + \frac{r_{cont}}{r_i}}{\sin^{-1}\left(\frac{r_{eff}}{r_i}\right) - \sin^{-1}\left(\frac{r_{cont}}{r_i}\right)}\right) + r_j\left(\frac{\sin^{-1}\left(\frac{r_{eff}}{r_j}\right) - \sin^{-1}\left(\frac{r_{cont}}{r_j}\right) - \frac{r_{eff}}{r_j} + \frac{r_{cont}}{r_j}}{\sin^{-1}\left(\frac{r_{eff}}{r_j}\right) - \sin^{-1}\left(\frac{r_{cont}}{r_j}\right)}\right). \quad 2\text{-}7$$

For the separated grain-wall pairs,

$$L_f = r_i\left(\frac{\frac{\pi}{2} - 1}{\frac{\pi}{2}}\right). \quad 2\text{-}8$$

Regarding the contacting grain-wall pairs,

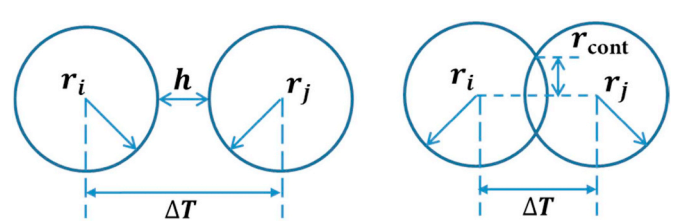

Fig. 1. Separated (left) and contacting (right) units.

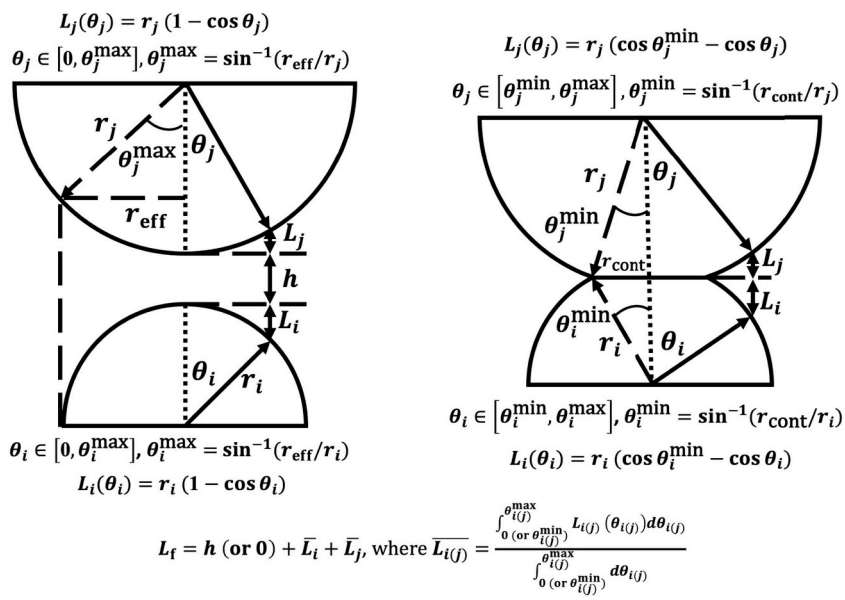

Fig. 2. Schematic drawings and brief derivation of L_f, Left – a separated unit with separation distance of h, and Right – a contacting unit with contact surface of r_{cont} in radius.

$$L_f = r_i\left(\frac{\frac{\pi}{2} - \sin^{-1}\left(\frac{r_{cont}}{r_i}\right) - 1 + \frac{r_{cont}}{r_i}}{\frac{\pi}{2} - \sin^{-1}\left(\frac{r_{cont}}{r_i}\right)}\right). \quad 2\text{-}9$$

With L_f computed by this method, the resulted Knudsen number Kn will be known, as well as the equivalent thermal conductivity k_g'. Eventually, $\alpha = k_g'/k_s$ will be used instead in Eqns. (2-1) and (2-2).

2.3. Limitation of the BOB model

In practical scenarios, the assumption of $\alpha \gg 1$ is not commonly satisfied, e.g., glass vs. air, implying that the realistic non-uniform temperature distribution within individual grains should not be neglected. Thereby, H_{cont} overestimates the heat conductance of individual contact units and thus the calculated k_{eff}/k_g. An empirical constant can be used to directly decrease k_{eff}/k_g [14] based on experimental data, but this is of little physical implication. To overcome this limitation, the non-uniform temperature distribution of grain $i\,(j)$ of one contact is simplified here as an equivalent temperature drop that is contributed by a cylindrical thermal resistor $R_{cyl.\,i(j)}$ [30] in the modified BOB model. Then, we make use of the thermal contact resistance $R_{cont} = 1/H_{cont}$, and the total thermal resistance of one contact unit is formulated as $R_{total} = R_{cont} + R_{cyl.\,i} + R_{cyl.\,j}$.

Assuming cylindrical thermal resistors having identical thermal conductivity k_s as grains, the thermal resistance of $R_{cyl.\,i(j)}$ is calculated according to their geometry as

$$R_{cyl.\,i(j)} = \frac{r_{i\,(j)}}{\pi\, k_s\,(\chi\, r_{eff})^2}, \quad 2\text{-}10$$

where r_{eff} is as defined in Section 2.2 and χ is the adjustable model parameter [30,42] mentioned in Section 2.1. We keep r_{eff} consistent with the implementation of Smoluchowski effect, although this definition is different from the previous one that $r_{eff} = r_{ij}$ used in Ref. [30]. The determination of χ becomes the essential step towards ensuring the accuracy of the modified BOB model. In the reported works adopting this model, χ is empirically fitted according to experimental data [28,30,46], revealing that χ is related to the thermal conductivity ratio α.

2.4. Determination of the model parameter χ

As discussed in the preceding section, χ is the only parameter to be

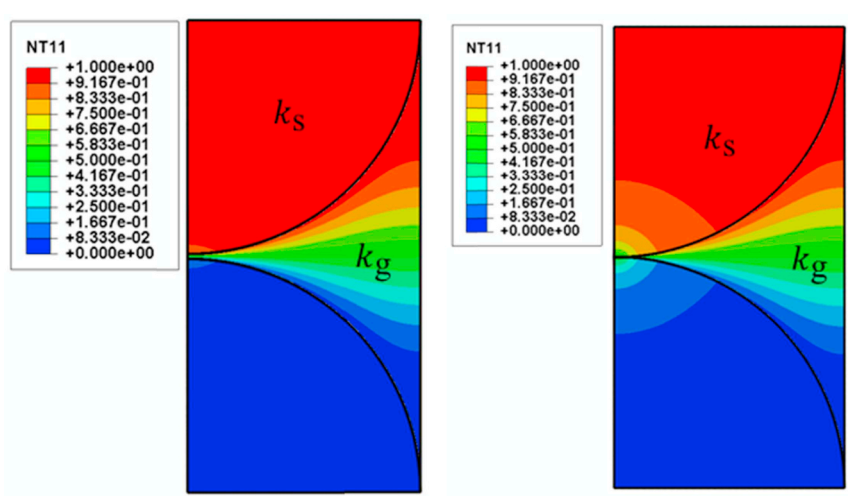

Fig. 3. Separated (left) and contacting (right) geometries coloured to show the steady state temperature field of the finite element simulation.

determined for intergranular heat transfer through contact units. In the literature, $\chi = 0.5$ is used for $\alpha = 120$ [30] and $\chi = 0.71$ is used for $\alpha = 10$ [28], both giving good agreement with experimental results. But it is prohibitively time consuming to collect experimental data across the entire range of α values, not to mention the associated measurement uncertainty. Thus, an estimation of χ is useful for prediction purposes. Here, finite element analysis (using ABAQUS software) is employed [18,47] to evaluate χ.

In finite element simulations, contact units, including both solid grains and gas phase, are assumed to be cylindrical, so axisymmetric modelling is used to reduce computational cost. Fourier's law is employed, and the steady-state simulation is selected in the analysis, as we consider only the steady state here. Two representative quadrants (solid) of $k_s = 100$ W/mK with the interstitial part (gas) of $k_g = k_s/\alpha$ form separated and contacting contact units in the simulations as shown in the left and right of Fig. 3, respectively. The radii of the quadrants are set to be $r_c = 1$ m and the separation distance h and the contact radius r_{cont} are varied to generate different geometries for simulations. These exact dimensions can be later normalised, because the material properties have no size-dependence. Particularly, the contact patch is created by truncating these quadrants to leave a specified contact radius. For a given radius, the height of the truncated quadrants differs slightly from that calculated by Hertzian contact mechanics (less than 0.1%), if the contact units are not severely compressed (indentation smaller than 0.2%).

The following procedure is carried out to numerically estimate χ. A constant temperature difference ΔT of 1K is imposed between the top and bottom surfaces of each contact unit while the axial boundaries are set to be adiabatic. The interfaces between solid and gas as well as between solid and solid are tied so no temperature difference exists in the simulation. α is varied from 10^6 to 4 because the original BOB model gives a contradictory trend when α is larger than 4. r_{cont}/r_c is varied from 0.0477 to 0.002 and h/r_c is varied from 0.000002 to 0.2. Examples of the simulated temperature fields are shown in Fig. 3. The total heat flow in the simulation Q_{FEM} passing through the top surface is extracted at steady-state and compared with the heat flow calculated based on the original BOB model Q_{BOB}. According to the relationship between total heat flow, temperature difference and thermal resistance, we have

$$\Delta T = R_{cont}\, Q_{BOB}, \qquad 2\text{-}11$$

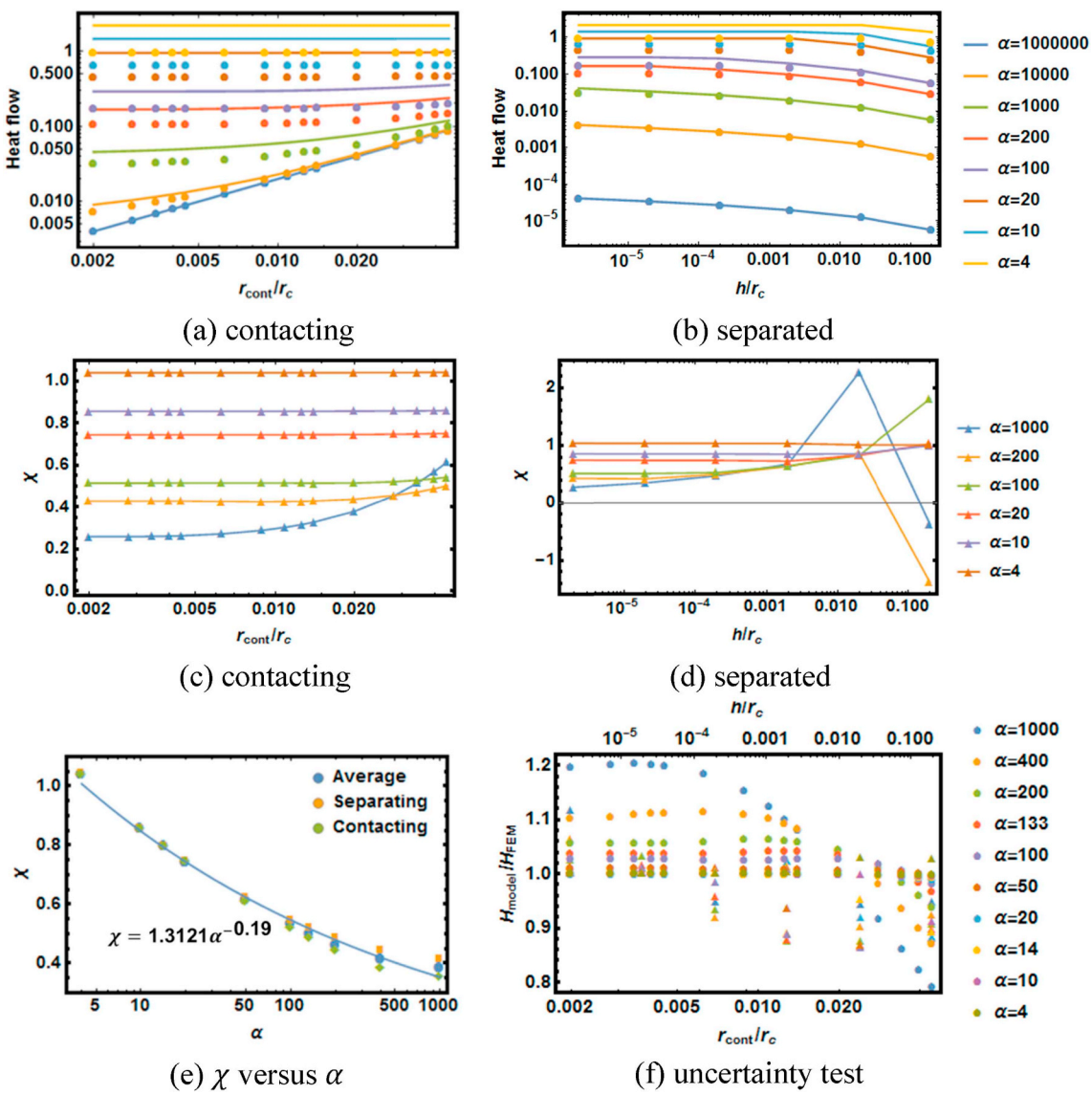

Fig. 4. (a) and (b) compare the heat flow between the finite element simulation (filled circles) and the original Batchelor & O'Brien model (solid lines), coloured according to α. (c) and (d) plot χ for each α and r_{cont}/r_c pair as well as α and h/r_c pair with joining lines, respectively. (e) gives the correlation between χ and α and (f) compares the computed heat flow between the modified model using the correlation in (e) and the simulated result.

$$\Delta T = (R_{\text{cont}} + 2\,R_{\text{cyl.}\,i})\,Q_{\text{FEM}}. \qquad 2\text{-}12$$

Replacing $R_{\text{cyl.}\,i}$ by Eqns. (2–10) and R_{cont} by Eqns. (2–11) in Eqns. (2–12), we found that χ can be evaluated by

$$\chi = \left[\sqrt{\left(\frac{\Delta T}{Q_{\text{FEM}}} - \frac{\Delta T}{Q_{\text{BOB}}}\right)\frac{\pi\,k_s\,r_i}{2}}\right]^{-1}. \qquad 2\text{-}13$$

In this work, the finite element analysis is considered to be more accurate than the original BOB model due to its capability to simulate temperature variation within grains. Both heat flows, Q_{BOB} and Q_{FEM}, are further nondimensionlised by a factor of $(\Delta T k_s r_i)$ in the following discussion. According to (a) and (b) in Fig. 4, the original BOB model shows fairly good accuracy for $\alpha \geq 10000$, but the overestimation turns out to be large when $\alpha \leq 1000$. Therefore, the evaluation of χ is mainly conducted in the α ranging from 1000 to 4. As shown in (c) and (d) in Fig. 4, For the contacting units, the variation of χ against r_{cont} becomes stable as $\alpha \leq 200$, implying the compression on the contact units has limited influence on χ in this condition. Although the model underestimates the heat flow and gives negative χ in the separated scenario when $\alpha \geq 200$, it occurs at relatively large h/r_c and results in small heat flow. Thereby, this negative part is neglected, and χ of corresponding α in both scenarios is comparable.

Regarding each α, the representative χ is calculated as the mean χ over all r_{cont}/r_c and h/r_c cases for contacting and separated units, respectively. It can be seen from (e) in Fig. 4 that χ exhibits similar values against α in both scenarios. Thus, the average χ of two scenarios is used, and finally a fitted power function against α gives,

$$\chi = 1.3121\,\alpha^{-0.19}. \qquad 2\text{-}14$$

The heat flow calculated by the modified BOB model with the proposed correlation presents reasonable agreement with the finite element simulation results, but large α reduces its accuracy, as shown in Fig. 4 (f). In the literature, χ is determined to be 0.5 for $\alpha = 120$ [30] and 0.71 for $\alpha = 10$ [28], while this method gives χ to be 0.528 and 0.846, respectively. The differences in the detail of the heat transfer models and polydispersity in those work contribute to the discrepancy. Nevertheless, this function is useful for predictive purposes, especially for conditions of $\alpha < 1000$. Although this function is derived purely based on monodispersed grains, we directly apply it for poly-dispersed granular media and test the reliability in latter sections.

To this end, the grain-scale heat transfer model can be summarised as a combination of the original BOB model, to obtain H_{cont} by Eqns. (2)–(1) and Eqns. (2)–(2), and a compensation function of thermal resistance, to calculate $R_{\text{cyl.}\,i(j)}$ using the correlation between χ and α. In summary, for a given contact unit comprising grains i and j whose temperature difference is ΔT, the heat flow Q_{ij} passing through this unit can be computed according to

$$Q_{ij} = \Delta T\left[\frac{1}{H_{\text{cont}}(h,\ r_{\text{cont}},\ \alpha,\ r_i,\ r_j)} + R_{\text{cyl.}\,i}(\chi(\alpha),\ r_i) + R_{\text{cyl.}\,j}(\chi(\alpha),\ r_j)\right]^{-1}. \qquad 2\text{-}15$$

2.5. Simulation protocol

The grain-scale heat transfer model of individual contact units, represented by Eqns. (2–15), is coded in C++ within LIGGGHTS framework (DCS Computing GmbH). The mechanical behaviour is determined by Hertzian contact mechanics, and the heat transfer processes are computed by iterating the temperature of each grains according to their heat capacity and overall heat flow based on contact units and Eqns. (2–15). In addition, a cut-off value h_{cutoff} is used to avoid counting unnecessary contact units in the DEM simulation. It has been shown that $\varepsilon = 0.5$ in $h_{\text{cutoff}} = \varepsilon\,r_{ij}$ is suitable for general consideration [44].

For each simulation, a granular medium will be generated in a given geometry that should have a uniform cross-sectional area along the principle axis of temperature gap and specified boundaries in other axes according to simulation requirements. Following grains settling under gravitational force into a particular geometry, two flat walls which are set as a heat source and a heat sink with a constant temperature gap ΔT_{gap} of 1K are applied onto the principle axis. In addition, they can move along the same axis and press the granular medium. When target

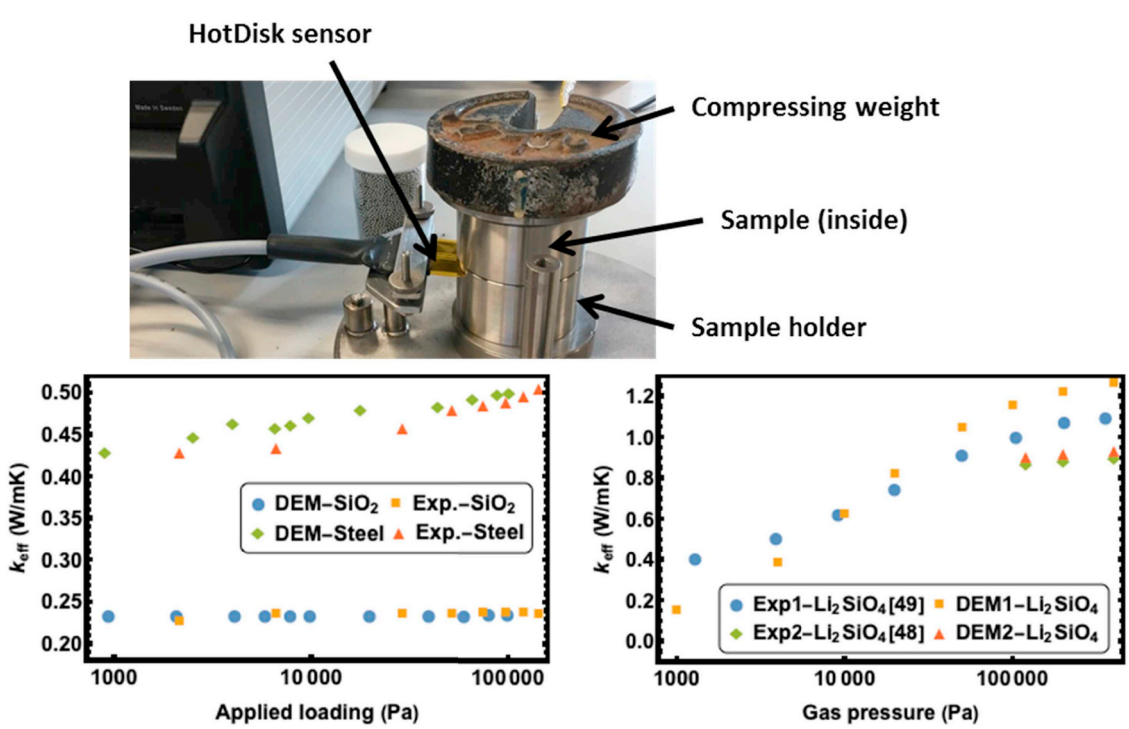

Fig. 5. Top – Experimental configuration. Bottom – Comparison between simulation results and the experimental measurement in this work (left) and previously published studies (right).

compression is achieved, the granular medium and two walls are frozen, and adiabatic condition are imposed in other boundaries. The granular medium is then heated until steady-state where the fractional difference between inflow heat and outflow heat is smaller than 10^{-6}. Finally, the effective thermal conductivity k_{eff} is expressed as

$$k_{\mathrm{eff}} = \frac{Q_{\mathrm{inflow}}\, L_{\mathrm{axis}}}{A_{\mathrm{cross-section}} \times \Delta T_{\mathrm{gap}}}, \qquad 2\text{-}16$$

where Q_{inflow} indicates the inflow heat, and L_{axis} and $A_{\mathrm{cross-section}}$ are respectively the length and the cross-sectional area of the granular medium. Alternatively, k_{eff} can be calculated also as

$$k_{\mathrm{eff}} = \frac{Q_{\mathrm{inflow}}}{A_{\mathrm{cross-section}}} \times \frac{1}{\Delta T_{\mathrm{gradient}}}, \qquad 2\text{-}17$$

with $\Delta T_{\mathrm{gradient}}$ representing the temperature gradient inside the granular medium. In general, by binning the grains according to their position in the principle axis, a linear function can be fitted based on the mean temperature of each bin against the corresponding representative position. Thus, $\Delta T_{\mathrm{gradient}}$ can be calculated as the slope of that linear function. Compared with the former expression, using $\Delta T_{\mathrm{gradient}}$ can exclude the wall-grain contacts and gives the more inherent k_{eff} of the granular medium. However, the former one is considered more appropriate for experimental validation as practical measurement always includes wall-grain contacts.

3. Experimental validation and discussion

The HotDisk system built with a transient plane source technique [48,49] is deployed to experimentally measure the effective thermal conductivity of granular media. A cylindrical load-bearing sample holder, shown in Fig. 5, is specifically designed to incorporate the mechanical influence on effective thermal conductivity. Two kinds of grains, 2 mm glass (k_s = 1.2 W/mK, Young's modulus = 63 GPa, Poisson ratio = 0.2) beads and 2 mm 304 stainless steel (k_s = 16.2 W/mK, Young's modulus = 200 GPa, Poisson ratio = 0.27) beads, are used separately to form solid-gas media in ambient air of atmospheric pressure and room temperature (k_g = 0.026 W/mK). The air properties are described by the correlations shown in Table 1.

Measurement results, shown in the bottom left of Fig. 5, reveal that the thermal transport of the two granular systems responds differently to mechanical loading. The effetive thermal conductivity of granular medium consisting of steel grains increases gradually with load, while the k_{eff} of the packed glass beads is insensitive. This difference can be understood considering steel has a thermal conductivity more than ten times higher than that of glass. The greater heat conduction pathways resulted from large load creating large contact areas have greater significance in the more thermally conductive steel, although glass has even larger contact areas in a similar condition. DEM results extracted from simulated granular media of similar geometry and volume as the experiments show quantitatively agreement with the measurement, proving the applicability of the model implementation introduced in Section 2.

The influence of the Smoluchowski effect and poly-dispersed size distributions are also examined with reference to published experimental results. A poly-dispersed granular medium of 20,000 grains of lithium orthosilicate Li_4SiO_4 [50] (k_s = 2.57 W/mK at 20 °C and k_s = 2.15 W/mK at 500 °C, Young's modulus = 88 GPa, Poisson ratio = 0.24) with helium filling (properties given in Table 1) is fed to the simulation of periodic boundary conditions. k_{eff} of the simulated media closely matches experimental data including gas pressure dependence. It should be pointed out that this heat transfer simulation slightly overestimates k_{eff} despite neglecting thermal radiation [51].

4. Result and discussion – effective thermal conductivity vs. packing structure

The roles of material properties and grain-grain interactions in overall thermal transport have been examined through the implementation of the discrete element simulation reported here and widely reported in the literature. Therefore, the following sections focus on establishing relationships between packing order and effective thermal conductivity.

4.1. Packing structure transition by vibration

It has been demonstrated that mechanical vibration can effectively change the packing structure of granular media [52]. For granular media settling freely under gravity, random disordered packing structures form with a few clusters of hexagonal-close-packed (HCP) and face-centred-cubic (FCC) packings. By vibration agitating granular media, disorder-to-order transitions are stimulated. Grains gradually rearrange themselves into structured clusters to achieve dynamic efficiency [40,53]. Not only can the packing fractions be varied, but also the order levels of the packing structures significantly increase during vibration. The vibration protocol used in this study is as follow: granular media with a constant number of grains are generated by a free-falling method within finite cylinders of varying diameters under gravitational force that is applied along the axial direction of these cylinders in LIGGGHTS; these packings are then subjected to continuous mechanical vibration of sine wave agitation by the bottom surface at frequency of 50 Hz in anti-gravitational direction with amplitude of 0.46 mm (1/5 of the diameter of grains in the simulation) for 1000 periods; and as a result, excited grains relocate into new positions, forming ordered and quasi-equilibrium states [53]. Three types of granular media are simulated, and their geometrical dimensions are summarised in Table 2. For each geometry, five samples are extracted at different vibration durations for subsequent heat transfer simulation.

To quantify this disorder-to-order transition, the structural index S_6 that measures the rotational symmetry of the neighbour configuration of granular media is used. In such measurements, the neighbour configuration of each grain is first represented by a vector, and then the cosine similarity between the vector of a particular grain and those vectors of its neighbour grains is used to evaluate the resemblance between the neighbour configurations of these grains (a detailed procedure is given in the Appendix). Thus, the order level of grain-scale packing structure is positively described by the aforementioned resemblance, with values ranging from 0 to 12 [38,53,54]. Voronoi tessellation [55] is employed to obtain the effective volume V_V of each grain by splitting the total volume of given granular media, and packing fraction φ_V of individual grains can be calculated according to $\varphi_V = V_{\mathrm{sphere}}/V_V$. In this way, the mean values of S_6 and φ_V, excluding surface grains, can be recognised as the global characteristics of a granular medium. As shown in Fig. 6, the mean values of both of S_6 and φ_V monotonically increase with vibration, which implies a cooperative

Table 1
Gas properties used in this work.

Gas type	Properties	
Helium (He)	k_g / (W/mK):	$3.366 \times 10^{-3} T^{0.668}$ (T in K).
	d_g / (m):	2.15×10^{-10}.
	m_g / (g/mol):	4.
Air	k_g / (W/mK):	$-10^{-11}T^3 - 4\times10^8 T^2 + 8\times10^5 T + 0.0241$ (T in °C).
	d_g / (m):	3.66×10^{-10}.
	m_g / (g/mol):	28.96.

Table 2
Geometry parameters of granular media.

Diameter of grain	2.3 (mm)
Number of grains	5000
Cylinder Diameter/Height	30/75, 40/60, 50/25 (mm/mm) denoted as D30, D40, D50

process between densification and ordering in granular media and further demonstrated in the right of Fig. 6. The reason for the sudden increase of φ_V in D50 can be explained by the geometrical effect in the ordering process [53]. The large cylinder diameter promotes the growth of perfect HCP and FCC clusters, while the small one causes distortion in the ordered clusters with imperfection.

By considering individual grain positions, the spatial resolution of S_6 can be further revealed. Due to the symmetry of the cylindrical containers, two-dimensional (2D) radial sections are studied and sub-domains are created by mapping a 2D grid with grain diameter resolution onto these sections. By sweeping the cylindrical spaces with the 2D sections, grains are mapped into the relevant sub-domains according to their radial distance x_{radial} and height z, and then the mean S_6 of each sub-domain can be obtained to yield intensity maps of S_6. Spatial patterns of these maps are found to be nearly axisymmetric. A typical evolution of S_6 distribution is shown in Fig. 7 presenting a spatially inhomogeneous order development.

4.2. Enhanced effective thermal conductivity by vibration

To examine the role of packing structure in thermal conductivity we consider a medium consisting of glass (SiO_2) grains filled with a gas phase of helium (He). By varying the helium pressure in the simulation, α can be varied over a large range for a given solid phase. According to Fig. 8 (a), the Smoluchowski effect strongly influences the thermal conductivity of He in the pressure range from 1Pa to 10^5 Pa and brings about a change in α roughly from 10^4 to 10, respectively. In considering the correlation between χ and α, helium pressures of 10 Pa, 10^2 Pa, 10^3 Pa, 10^4 Pa and 10^5 Pa are used. To avoid floating grains, granular media are initially compressed by a mechanical loading of 1 MPa in the simulations.

By using the fitted $\Delta T_{\text{gradient}}$ in Eqns. (2–17), the boundary effect is subtracted and a more inherent value of k_{eff} can be obtained in the following sections. Firstly, correlations between k_{eff} and the global φ_V as well as between k_{eff} and the global S_6 are studied. In Fig. 8(b) and (c) show plots of the maximum α ($\approx$ 1000) while (d) and (e) are extracted from the minimum α (<10). A collective correlation between k_{eff} and the global φ_V of different samples can be observed for large α, but the correlations split at small α values. In contrast, correlations between k_{eff} and the global S_6 tend to converge for small α but diverge for large α. This difference indicates that the corresponding influences of densification and ordering are gradually weakened and strengthened, respectively, as α decreases. Besides, the unusual drop and jump in (b) and (c) should be clarified. The breakdown of the monotonic increase of k_{eff} against φ_V is considered to be the result of insufficient contact between the heat source wall and boundary grains in the simulation, leading to poorer heat transfer into the media. However, this influence becomes insignificant when α is small.

This global observation indicates that neither packing fraction nor structure order can determine k_{eff} alone. The collective processes of densification and ordering are the reason for the enhancement of k_{eff} introduced by vibration. But, by decreasing α, the prominence in such processes shifts from packing fraction to structure order.

4.3. Grain-scale structure and heat transfer

It has been shown that k_{eff} of granular media is positively correlated to both φ_V and S_6 at the macroscale, but mechanisms at finer scales are insufficiently understood. As demonstrated in Fig. 7, the structural transition brings about substantial and inhomogeneous grain-scale ordering. Whether this improvement of order enhances heat transfer in granular media and if so, how this enhancement works remains elusive. To address this interplay between grain-scale structure and thermal transport, analysis of heat transfer at the grain-scale is performed as following.

Analytically, a heat flow density vector $\boldsymbol{Q}_{\text{density}}$ across the surface of an individual grain in a granular medium can be presented as [14],

$$\boldsymbol{Q}_{\text{density}} = n \sum_i \boldsymbol{x}_i Q_i \,, \tag{4-1}$$

where Q_i is the heat flow passing through each contact, $\boldsymbol{x}_i$ is the vector pointing from the centroid of the particular grain toward the corresponding contact point and n is the individual grain number density, the reciprocal of the Voronoi volume of the corresponding grain $1/V_V$ [55]. It has also been proved that the temperature gradient vector of each grain is equal to the global temperature gradient vector $\Delta\boldsymbol{T}_{\text{gradient}}$ of the entire granular medium [14]. Based on this consideration, an expression is validated for each grain,

$$\boldsymbol{Q}_{\text{density}} = \boldsymbol{k}^* \, \Delta\boldsymbol{T}_{\text{gradient}} = n \sum_i \boldsymbol{x}_i Q_i \,, \tag{4-2}$$

with $\boldsymbol{k}^*$ being the second rank thermal conductivity tensor for each grain. Therefore, $\boldsymbol{k}^*$ of individual grains can be derived by knowing their neighbour configurations and the corresponding inter-grain heat flows that can be easily extracted from DEM. Besides, the sum of heat flows of each grain is 0 at steady-state, $\sum_i H_i = 0$, so by summing either inflow or outflow heat for each grain, the scalar quantity of total heat flow Q_{flow} through one grain can also be calculated. In such measurements, two aspects of heat transfer at the grain-scale can be investigated, the magnitude of the heat flow and the directional thermal conductivity. The fitted $\Delta T_{\text{gradient}}$ in Eqns. (2–17) is used and resulted in $\Delta\boldsymbol{T}_{\text{gradient}} = \{0,\ 0,\ \Delta T_{\text{gradient}}\}$ in accordance with the imposed temperature boundary condition. Because of this uni-directional temperature gradient, only the z component of thermal conductivity tensor $\boldsymbol{k}^*$ is needed, $\boldsymbol{k}^*_z = \{k_{zx},\ k_{zy},\ k_{zz}\}$. The principle component k_{zz} is of most interest, and the anisotropy $\theta_z = \text{ArcCos}(k_{zz}/|\boldsymbol{k}^*|_z)$ of this $\boldsymbol{k}^*_z$ is also examined.

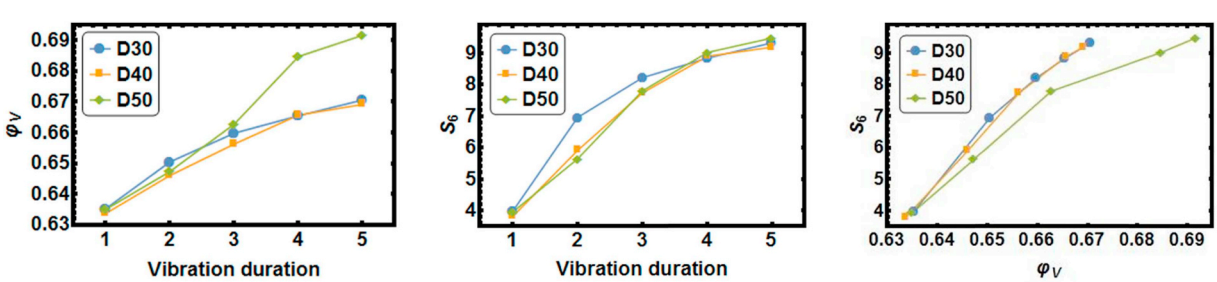

Fig. 6. φ_V (– left) and S_6 (– middle) increase as the duration of vibration is extended, noticing that the horizontal axis is arbitrary. S_6 vs. φ_V (– right) demonstrates the cooperative process.

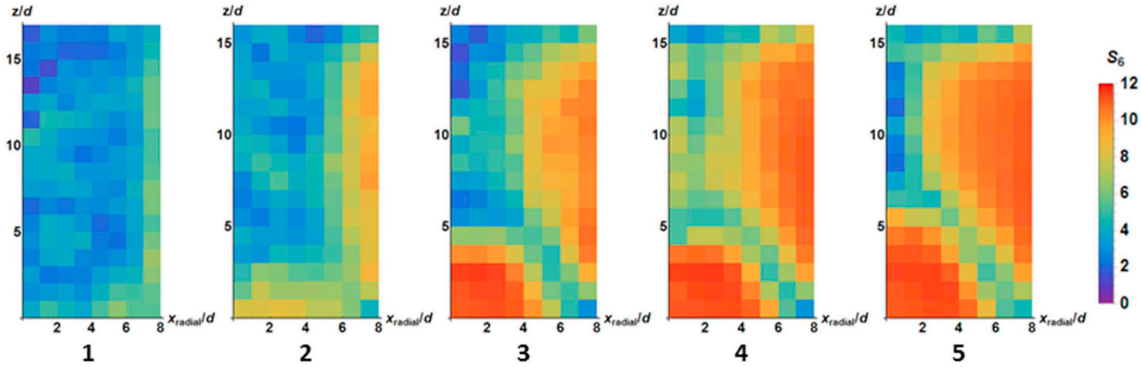

Fig. 7. Evolution of S_6 spatial patterns in D40 with vibration duration (from left to right).

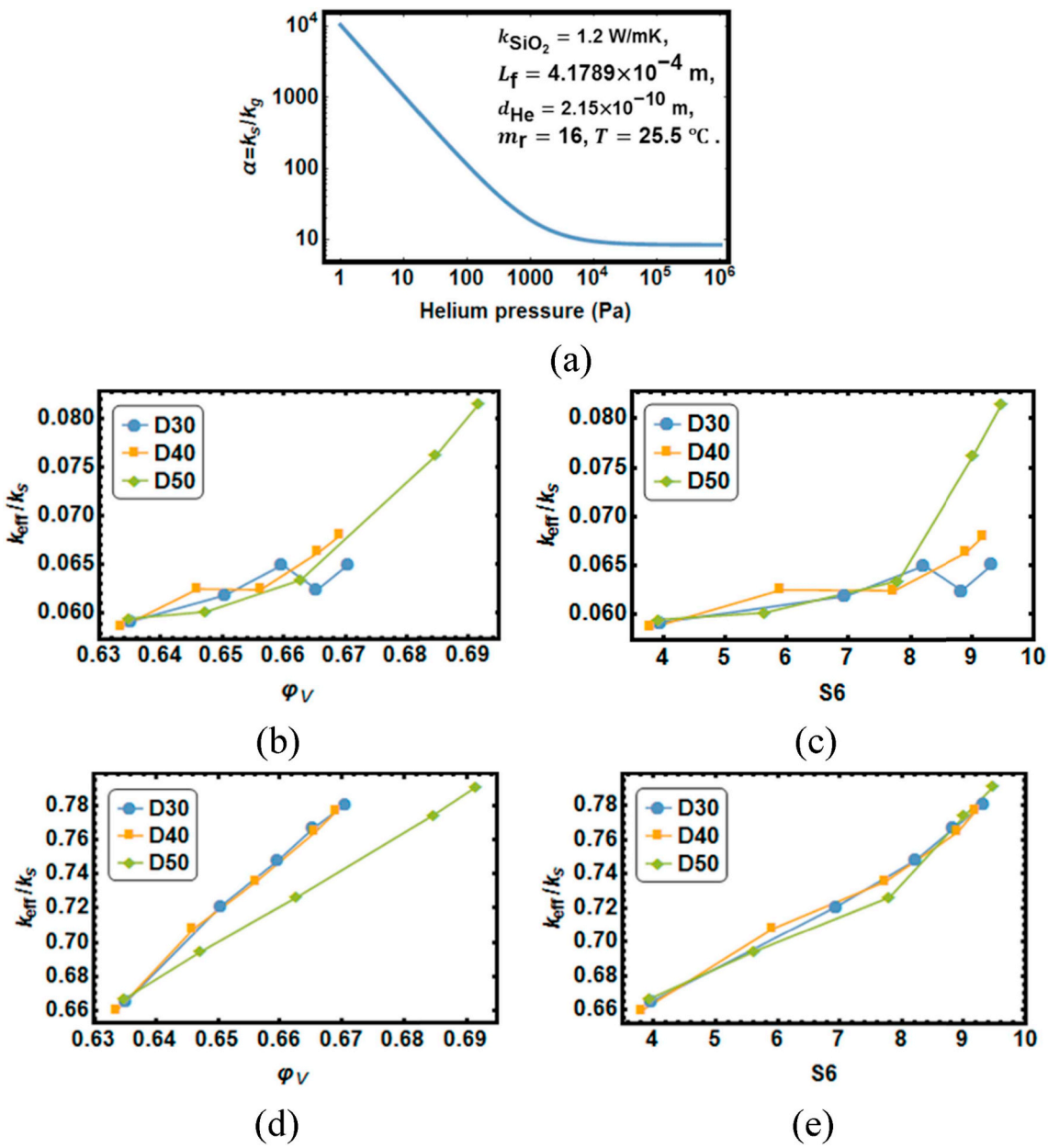

Fig. 8. (a) The variation of α with helium gas pressure in SiO_2-He granular media consisting of 2.3-mm-diameter SiO_2 grains at room temperature according Section 2.2. (b) and (c) show the correlations of (k_{eff}, φ_V) and (k_{eff}, S_6) in the maximum α ($\approx$ 1000), respectively. (d) and (e) show the same types of correlations of the minimum α (<10). All are extracted from DEM simulation.

A similar analysis to that presented in Fig. 7 is applied to examine the spatial distributions of the thermal conductivity tensor k_{zz}, its anisotropy θ_z and the grain level heat flow Q_{flow}. The spatial evolution of the ratio k_{zz}/k_s and θ_z for a D40 sample with $\alpha \approx 10$ is shown sequentially in the top and middle rows of Fig. 9, respectively. The spatial distribution of k_{zz}/k_s correlates positively to that of S_6 in Fig. 7, while θ_z exhibits inverse patterns. In contrast, the spatial distribution of non-dimensional Q_{flow} (bottom row in Fig. 9) does not show any observable trend that can be correlated to structural patterns, and only exhibits a globally increasing trend along with the enhancement of overall S_6. This suggests that k_{zz} and θ_z are closely related to the grain-scale structure, but Q_{flow} is less influenced.

Comparing the evolution of the spatial distributions of k_{zz}/k_s and θ_z with the evolution of S_6, it can be seen that, at the grain-scale, ordering increases thermal conductivity and decreases anisotropy, resulting in similar inhomogeneous spatial patterns. In fact, due to the cooperativity of the densification and ordering, the spatial patterns of φ_V are nearly identical to those of S_6. Thus, it is hard to differentiate the influences of these two processes, but ordering is considered to be precedence of densification in vibrated granular media due to the rigidity of grains. However, it is clear that the decrease of anisotropy, θ_z, can be related to a greater symmetry of the neighbourhood configurations of individual grains, which is specifically measured by S_6. Further, the bottom ordered region in the patterns of Fig. 7 exhibits a higher k_{zz}/k_{eff} and lower θ_z in Fig. 9 than the corresponding side ordered region. This contrast can be attributed to the different completeness of ordering in these two regions. As mentioned before, due to the curved cylinder wall, distortion occurs in the side region [53], making the ordered packing structures deviate from perfect FCC and HCP and become looser as well as less symmetric. In summary, two grain-scale mechanisms to enhance the macroscopic k_{eff} are identified regarding to the ordered packing structure.

By transforming the quantitative results from the mapping operations of Figs. 6 and 9 into the coordinate plots shown in Fig. 10, the Pearson correlation coefficient is employed to evaluate the correlations of (S_6, k_{zz}) and (S_6, θ_z) in the left and middle of Fig. 10, respectively. It confirms the positive correlation between S_6 and k_{zz} together with the negative correlation between S_6 and θ_z. However, such correlations become stronger as the diameter of the granular media increases. The reason for this augmentation can be understood by considering the aforementioned differences in the structured regions; because the packing structures formed in D30 are dominated by distorted HCP structures [53] while D50 consists of perfectly ordered structures. In addition, the correlation between φ_V and k_{zz} is found to give the highest Pearson correlation coefficient, although this is unsurprising as φ_V is used in the calculation of k_{zz} in Eqns. (4)–(2).

The influence of α observed in Fig. 8 is further examined by this method. The (S_6, k_{zz}) and (S_6, θ_z) are plotted in Fig. 11 for well-structured granular media following the final vibration time. That lower values of α enhance the various correlations can be found here. This enhancement arises as the reduction of α enlarges the effective volume of gas phase participating in heat transfer at contacts, achieving a more homogeneous heat flow profile on grain surfaces and compensating for the structural distortion that arises from the cylindrical boundary. This effect can be implied from the contrast between (b) and (d) in D30 and D40 samples, especially the significant decreases of θ_z, as the α drops from 1000 to 10. Due to the relatively poor order of the side region in D50 samples regions [53], the compensating effect by the decrease of α becomes less effective. This discussion indicates an appropriate interpretation of the order of packing structure is necessary in the prediction of k_{eff} of granular media with small α.

Finally, it is necessary to point out that untangling the effects of

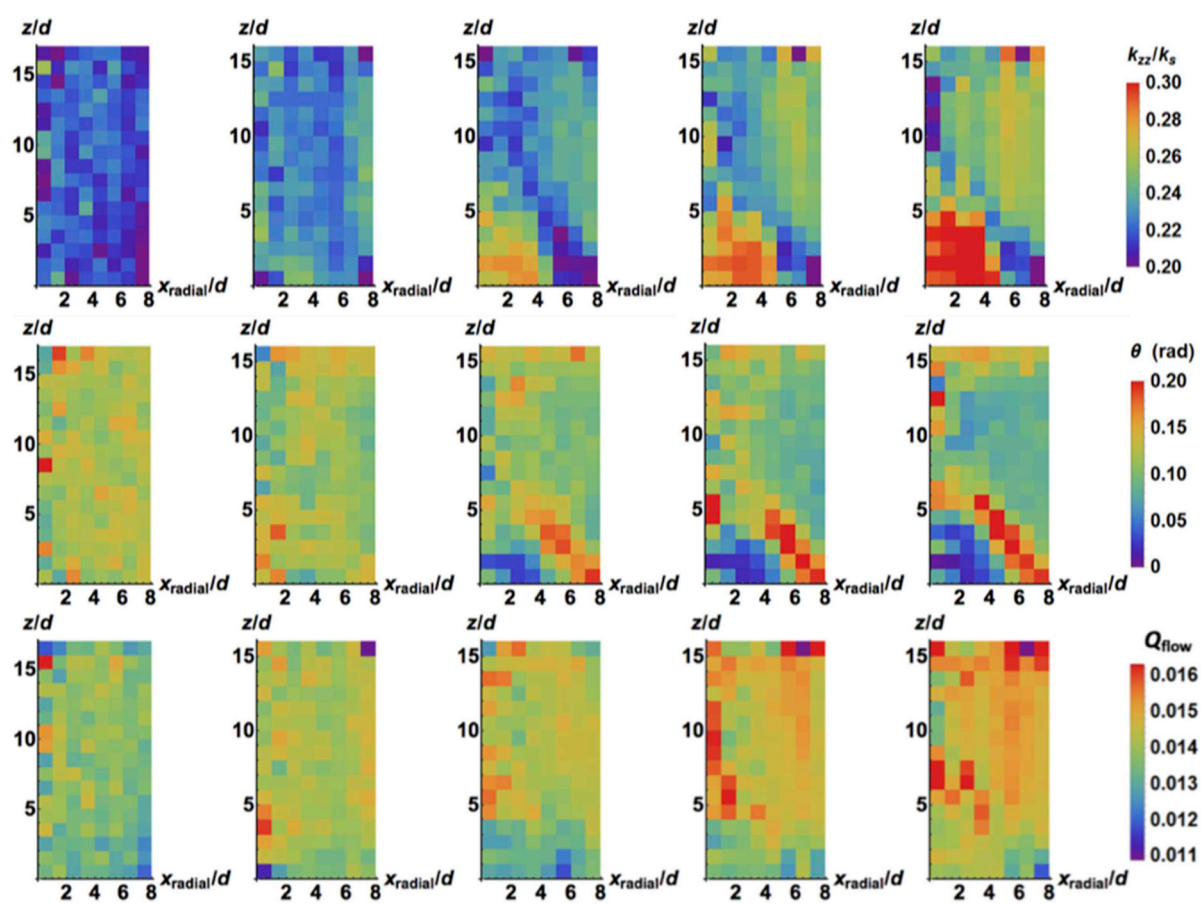

Fig. 9. Spatial evolution of k_{zz}/k_s (top row), θ_z (middle) and Q_{flow} (bottom) of the D40 granular media with packings of different order, increasing from left to right.

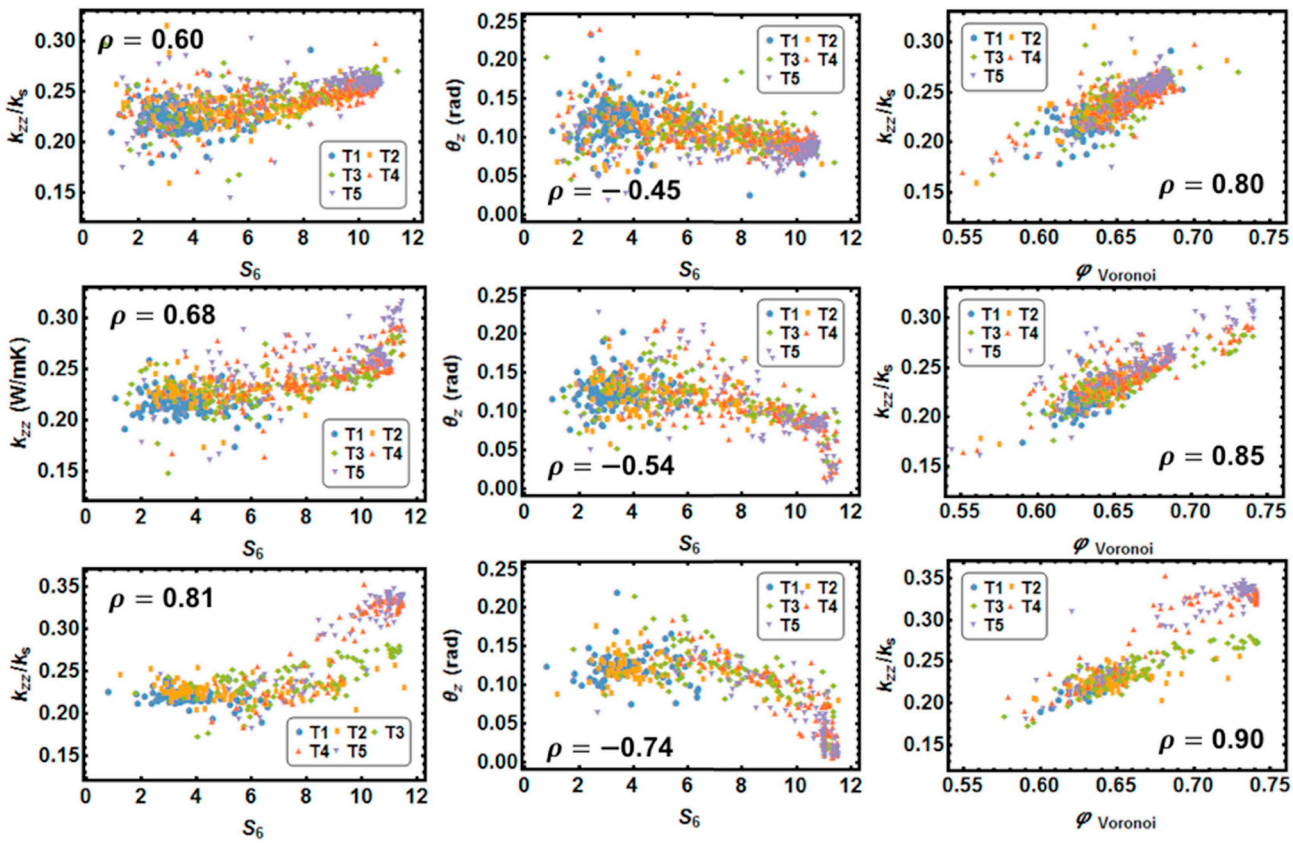

Fig. 10. Left – (S_6, k_{zz}), middle – (S_6, θ_z) and right – (ϕ_V , k_{zz}) plots of D30, D40 and D50 (from top to bottom respectively) according to the mapping operation, in the scenario of $\alpha = 100$.

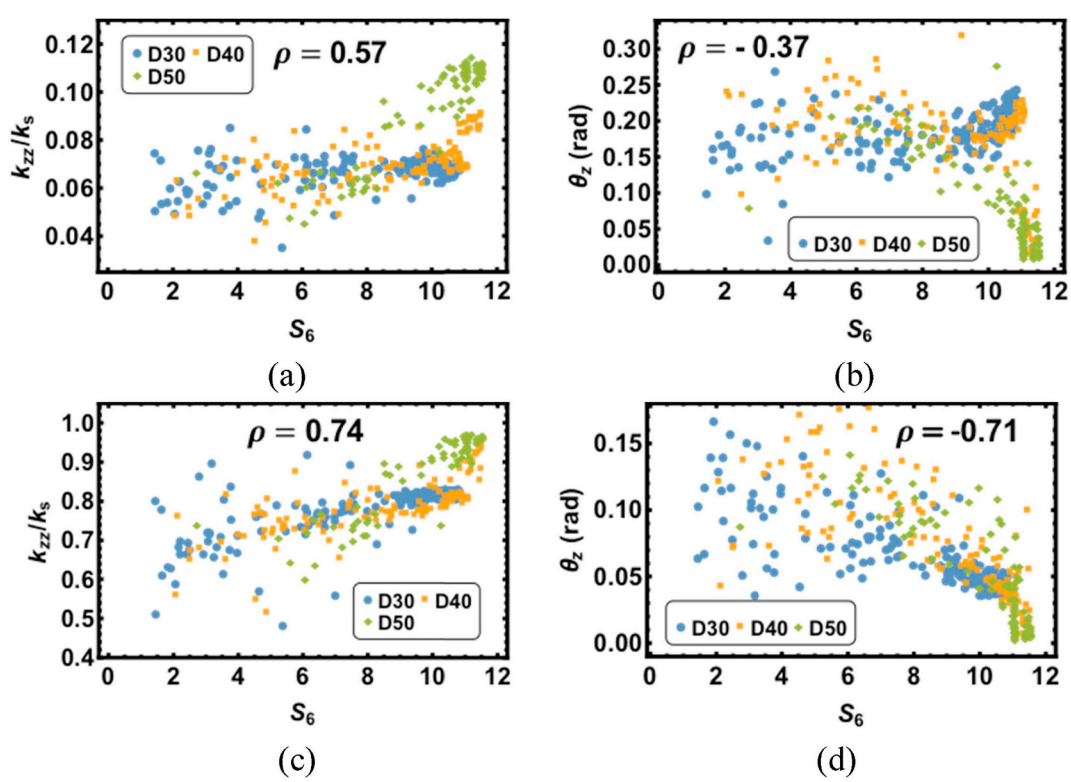

Fig. 11. (S_6, k_{zz}) and (S_6, θ_z) plots of well-ordered packing structures belonging to three types of granular media in different scenarios. (a) and (b) – $\alpha \approx 1000$, (c) and (d) – $\alpha \approx 10$.

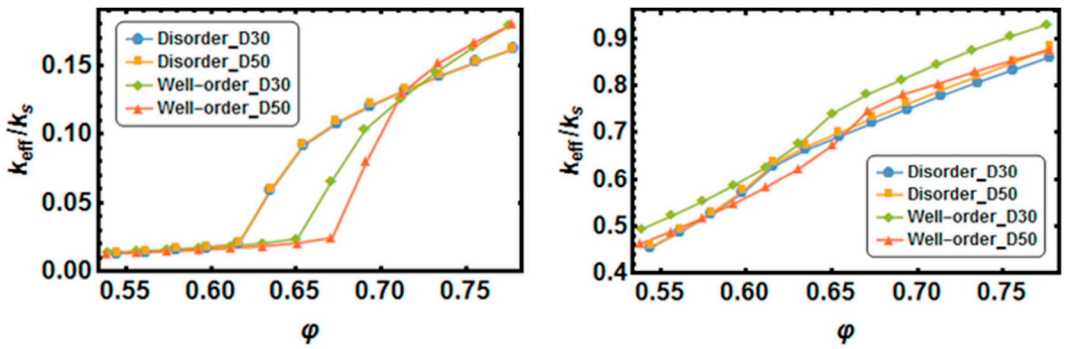

Fig. 12. The variation of k_{eff} with packing fraction in artificial media with disordered and well-ordered packing structures in $\alpha = 1000$ (left) and $\alpha = 10$ (right) scenarios.

packing ordering and densification is challenging in granular media. Nonetheless, an increase in local ordering can be clearly attributed to two results. One is the enhancement of grain-scale thermal conductivity along with the increase of packing fraction. The second is the reduction of anisotropy, improving the alignment of grain thermal conductivity with the principle heat transfer direction. Further, the effects of ordering could be more pronounced in systems where not all grains are in contact e.g. cemented granular media and grain-filler composites [19,56,57]. To check this point, the packing structures of those granular media are reused to form artificial grain-filled media. In these media, grains are fixed at the identical positions to maintain the order levels (disorder – initial state and well-order – longest vibrated state, corresponding to Fig. 6), but the radii of the grains are varied to adjust the packing fraction alone. As shown in Fig. 12, two scenarios of $\alpha = 1000$ (left) and $\alpha = 10$ (right) are presented, where the Smoluchowski effect is turned off to avoid the size dependency.

Firstly, despite the dissimilar tendencies of k_{eff} against φ in Fig. 12, a comparable shape of S can be identified. Although the S shape is flattened in the condition of $\alpha = 10$, the transition is still observed. This invariant occurrence of the transitions reflects the formation and loss of contacts between grains in corresponding to the change of packing fraction, i.e., the grain radius, which is the reason for the sharp transition in the condition of $\alpha = 1000$. The effect of the structural order depends upon α. In the large α condition, the ordered structures have relative uniform separation distance between grains, making the plunge of k_{eff} become sharper than the disorder structure as shown in the left of Fig. 12. But higher coordination number of the ordered structure improves the possibility of contact formation, resulting in higher k_{eff} with the packing fraction increasing. The mergence as the reduction of packing fraction in this scenario can be considered as the loose dispersion limit of the Maxwell model [7] where the structural order is least influential. However, when α is small, the preference between packing order and packing fraction further depends on the geometry. Due to the presence of the compensation by small α, the slender medium (D30) of ordered structure generally exhibits higher k_{eff} in the present packing fraction range. On the contrary, the flat medium (D50) presents similar change of the preference to that of $\alpha = 1000$. Such difference is attributed to the poorly ordered side region in D50 medium, which can also be recognised as the segregation of disordered regions. This segregation introduces disorder of larger dimension beyond the grain-scale, so out of the scope of current study.

5. Conclusion

In this work, a bi-phasic heat transfer model based on the Batchelor & O'Brien solutions has been successfully implemented in the open source software LIGGGHTS. In the current implementation, to overcome the limitation of the original model due to the assumption $k_s/k_g \gg 1$, a compensation method with only one model parameter χ is applied. With the help of finite element analysis of the heat transfer process of a series of contact geometries and k_s/k_g ratios, an empirical function is proposed to determine χ according to k_s/k_g for individual contacts. For a specific requirement in gas-solid granular media, the Smoluchowski effect is included in this modified model. Finally, this heat transfer simulation framework is validated by experimental measurements deploying a transient plane source technique as well as comparison with literature data. The simulated results show good agreement with mono-dispersed granular media, and the applicability for poly-dispersed granular media has also been tested, although further tests are required to characterise the uncertainty. As thermal radiation and convection have been ignored, this framework is optimal for granular media with stagnant gas phases at room temperature.

Granular media comprising glass and helium with different packing structures are applied in this heat simulation framework to study how the order characteristics of packing structures affect the effective thermal conductivity of these media. By investigating thermal properties and order characteristics at the grain-scale, it has been demonstrated that the structural disorder-to-order transition enhances the overall thermal conductivity k_{eff}. Locally, the increase of thermal conductivity in the principal direction k_{zz}, and the decrease of anisotropy θ_z, are further identified as outcomes of the structural transition resulting from grain-scale ordering processes. The heat flow through individual grains, Q_{flow}, is found to correlate strongly with the global structural variation but does not exhibit a clear relationship with local structure. The two grain-scale effects are further influenced by the k_s/k_g ratio. The findings here provide a potential method to manage heat transfer in granular media by manipulating packing structures and a conceptual framework for broader analysis of transport phenomena in granular media to fill the gap between micro-scale mechanisms and macro-scale phenomena.

Acknowledgements

This work was financially supported by Australian Research Council (Projects DE130101639 and DP170102886) and The University of Sydney SOAR Fellowship.

Appendix

The Structural index S_6 [58] is based on the bond orientation parameters [59] and can be calculated the following procedure [53,54]. The bond orientation order parameters, initially defined by Steinhardt *et al* [59], represent the rotational symmetry of sphere assemblies. For each bond $\vec{r}$ that is defined as a vector pointing from the centroid of a central particle to one of its neighbour particles, we have

$$Q_{lm}(\vec{r}) \equiv Y_{lm}(\theta(\vec{r}), \varphi(\vec{r})), \tag{S1}$$

where $\theta(\vec{r})$ and $\varphi(\vec{r})$ are the polar and azimuthal angles of the bond in a specific spherical coordinates system, $Y_{lm}(\theta, \varphi)$ is spherical harmonics and l and m are integers indicating the order of spherical harmonics with the condition that $l \geq 0$ and $|m| \leq l$. By averaging $Q_{lm}(\vec{r})$ over the n_b^i closest neighbours of a central sphere i, the following expression is obtained,

$$\hat{q}_{lm}(i) = \frac{1}{n_b^i} \sum_{k=1}^{n_b^i} Q_{lm}^{i,k}(k). \tag{S2}$$

Considering a sphere can have a maximum of 12 neighbours of identical spheres forming point contacts, we select $n_b^i = 12$, which is also a common practice [54]. The neighbourhood configuration of a central sphere i can be further represented by a vector $\vec{\boldsymbol{q}}_6(i) = [\hat{q}_{6m}(i)]$, with $m = -6, -5, ...0, ...5, 6$ [58]. The cosine similarity $CosSimi(i, j)$ of a pair of such vectors of neighbouring spheres i and j is calculated as

$$\mathrm{CosSimi}(i, j) = \mathbf{Re}\left[\frac{\vec{\boldsymbol{q}}_6(i)}{|\vec{\boldsymbol{q}}_6(i)|} \cdot \frac{\vec{\boldsymbol{q}}_6(j)}{|\vec{\boldsymbol{q}}_6(j)|}\right] = \mathbf{Re}\left[\frac{\sum_{m=-6}^{6} \hat{q}_{6m}(i) \cdot \hat{q}_{6m}^*(j)}{|\vec{\boldsymbol{q}}_6(i)||\vec{\boldsymbol{q}}_6(j)|}\right], \tag{S3}$$

to positively characterise the similarity of their individual neighbourhood configurations, ranging from 0 to 1. Hence, the structural index of a sphere i, S_6^i, can be considered as the degree of such similarity and represented by

$$S_6^i = \sum_{j}^{n_b^i} \mathrm{CosSimi}(i, j). \tag{S4}$$

The overall structural index of a granular medium S_6 can be defined as the mean of S_6^i.

Appendix A. Supplementary data

Supplementary data to this article can be found online at https://doi.org/10.1016/j.ijthermalsci.2019.04.028.

References

[1] Y. Gan, Francisco Hernandez, Dorian Hanaor, Ratna Annabattula, Marc Kamlah, Pavel Pereslavtsev, Thermal discrete element analysis of EU solid breeder blanket subjected to neutron irradiation, Fusion Sci. Technol. 66 (2014) 83–90.
[2] R. Dayal, T. Gambaryan-Roisman, Heat transfer in granular medium for application to selective laser melting: a numerical study, Int. J. Therm. Sci. 113 (2017) 38–50.
[3] A. Hussain, I.H. Abidi, C.Y. Tso, K.C. Chan, Z. Luo, C.Y.H. Chao, Thermal management of lithium ion batteries using graphene coated nickel foam saturated with phase change materials, Int. J. Therm. Sci. 124 (2018) 23–35.
[4] P. Richard, M. Nicodemi, R. Delannay, P. Ribiere, D. Bideau, Slow relaxation and compaction of granular systems, Nat. Mater. 4 (2005) 121–128.
[5] A.M. Abyzov, A.V. Goryunov, F.M. Shakhov, Effective thermal conductivity of disperse materials. I. Compliance of common models with experimental data, Int. J. Heat Mass Transf. 67 (2013) 752–767.
[6] O.B. Kovalev, A.V. Gusarov, Modeling of granular packed beds, their statistical analyses and evaluation of effective thermal conductivity, Int. J. Therm. Sci. 114 (2017) 327–341.
[7] J.K. Carson, S.J. Lovatt, D.J. Tanner, A.C. Cleland, Thermal conductivity bounds for isotropic, porous materials, Int. J. Heat Mass Transf. 48 (2005) 2150–2158.
[8] N. Zhang, Z. Wang, Review of soil thermal conductivity and predictive models, Int. J. Therm. Sci. 117 (2017) 172–183.
[9] S. Yagi, D. Kunii, Studies on effective thermal conductivities in packed beds, AIChE J. 3 (1957) 373–381.
[10] X. Chen, M. Louge, Heat transfer enhancement in dense suspensions of agitated solids. Part I: Theory, Int. J. Heat Mass Transf. 51 (2008) 5108–5118.
[11] P. Zehner, E. Schlunder, Thermal conductivity of packings at moderate temperatures, Chem. Ing. Tech. 42 (1970) 933.
[12] C.T. Hsu, P. Cheng, I.W. Wong, Modified Zehner-Schlunder models for stagnant thermal conductivity of porous media, Int. J. Heat Mass Transf. 37 (1994) 2751–2760.
[13] C.T. Hsu, P. Cheng, K.W. Wong, A lumped-parameter model for stagnant thermal conductivity of spatially periodic porous media, J. Heat Transf. 117 (1995) 264–269.
[14] G.K. Batchelor, R.W. O'Brien, Thermal and electrical conduction through a granular material, Roy. Soc. Proc. A 355 (1977) 313–333.
[15] A.V. Gusarov, E.P. Kovalev, Model of thermal conductivity in powder beds, Phys. Rev. B 80 (2009) 024202(024201)-024202(024212).
[16] M. Bahrami, M.M. Yovanovich, J.R. Culham, A compact model for spherical rough contacts, J. Tribol. 127 (2005) 884–889.
[17] A.J. Slavin, V. Arcas, C.A. Greenhalgh, E.R. Irvine, D.B. Marshall, Theoretical model for the thermal conductivity of a packed bed of solid spheroids in the presence of a static gas, with no adjustable parameters except at low pressure and temperature, Int. J. Heat Mass Transf. 45 (2002) 4151–4161.
[18] W. Dai, S. Pupeschi, D. Hanaor, Y. Gan, Influence of gas pressure on the effective thermal conductivity of ceramic breeder pebble beds, Fusion Eng. Des. 118 (2017) 45–51.
[19] S. Corasaniti, F. Gori, Heat conduction in two and three-phase media with solid spherical particles of the same diameter, Int. J. Therm. Sci. 112 (2017) 460–469.
[20] W. van Antwerpen, C.G. du Toit, P.G. Rousseau, A review of correlations to model the packing structure and effective thermal conductivity in packed beds of mono-sized spherical particles, Nucl. Eng. Des. 240 (2010) 1803–1818.
[21] P.A. Cundall, O.D.L. Strack, A discrete numerical model for granular assemblies, Geotechnique 29 (1979) 47–65.
[22] S. Luding, K. Manetsberger, J. Müllers, A discrete model for long time sintering, J. Mech. Phys. Solids 53 (2005) 455–491.
[23] H.P. Zhu, Z.Y. Zhou, R.Y. Yang, A.B. Yu, Discrete particle simulation of particulate systems: a review of major applications and findings, Chem. Eng. Sci. 63 (2008) 5728–5770.
[24] Y. Gan, M. Kamlah, J. Reimann, Computer simulation of packing structure in pebble beds, Fusion Eng. Des. 85 (2010) 1782–1787.
[25] Y. Gan, M. Kamlah, Discrete element modelling of pebble beds: with application to uniaxial compression tests of ceramic breeder pebble beds, J. Mech. Phys. Solids 58 (2010) 129–144.
[26] W.L. Vargas, J.J. McCarthy, Heat conduction in granular materials, AIChE J. 47 (2001) 1052–1059.
[27] Y.T. Feng, K. Han, C.F. Li, D.R.J. Owen, Discrete thermal element modelling of heat conduction in particle systems: basic formulations, J. Comput. Phys. 227 (2008) 5072–5089.
[28] M. Moscardini, Y. Gan, S. Pupeschi, M. Kamlah, Discrete element method for effective thermal conductivity of packed pebbles accounting for the Smoluchowski effect, Fusion Eng. Des. 127 (2018) 192–201.
[29] G.J. Cheng, A.B. Yu, P. Zulli, Evaluation of effective thermal conductivity from the structure of a packed bed, Chem. Eng. Sci. 54 (1999) 4199–4209.
[30] T.S. Yun, T.M. Evans, Three-dimensional random network model for thermal conductivity in particulate materials, Comput. Geotech. 37 (2010) 991–998.
[31] C. Zhai, D. Hanaor, G. Proust, L. Brassart, Y. Gan, Interfacial electro-mechanical behaviour at rough surfaces, Extreme Mech. Lett. 9 (2016) 422–429.
[32] A.B. Yu, X.Z. An, R.P. Zou, R.Y. Yang, K. Kendall, Self-assembly of particles for densest packing by mechanical vibration, Phys. Rev. Lett. 97 (2006) 265501.
[33] K.J. Dong, R.Y. Yang, R.P. Zou, A.B. Yu, Role of interparticle forces in the formation of random loose packing, Phys. Rev. Lett. 96 (2006) 145505.
[34] X.Z. An, K.J. Dong, R.Y. Yang, R.P. Zou, C.C. Wang, A.B. Yu, Quasi-universality in the packing of uniform spheres under gravity, Granul. Matter 18 (2016) 1–7.
[35] E. Tsotsas, H. Martin, Thermal conductivity of packed beds- A review, Chem. Eng. Process 22 (1987) 19–37.
[36] J.J.M. Watson L. Vargas, Stress effects on the conductivity of particulate beds, Chem. Eng. Sci. 57 (2002) 13.
[37] M.X. Lim, R.P. Behringer, Topology of force networks in granular media under impact, EPL (Europhys. Lett.) 120 (2017) 44003.
[38] C.P. Goodrich, A.J. Liu, S.R. Nagel, Solids between the mechanical extremes of order and disorder, Nat. Phys. 10 (2014) 578–581.
[39] M. Hanifpour, N. Francois, S.M. Vaez Allaei, T. Senden, M. Saadatfar, Mechanical characterization of partially crystallized sphere packings, Phys. Rev. Lett. 113 (2014) 148001.
[40] J. Reimann, J. Vicente, E. Brun, C. Ferrero, Y. Gan, A. Rack, X-ray tomography investigations of mono-sized sphere packing structures in cylindrical containers, Powder Technol. 318 (2017) 471–483.
[41] M. Mirbagheri, R.J. Hill, Diffusion in sphere and spherical-cavity arrays with

interacting gas and surface phases, Chem. Eng. Sci. 160 (2017) 419–427.
[42] M. Mirbagheri, R.J. Hill, Sorption and diffusion of moisture in silica-polyacrylamide nanocomposite films, Polymer 122 (2017) 359–371.
[43] C. Kloss, C. Goniva, A. Hager, S. Amberger, S. Pirker, Models, algorithms and validation for opensource DEM and CFD-DEM, Prog. Comput. Fluid Dynam. Int. J. 12 (2012) 140–152.
[44] G.S. Sasanka Kanuparthi, Thomas Siegmund, Bahgat Sammakia, An efficient network model for determining the effective thermal conductivity of particulate thermal interface materials, IEEE Trans. Compon. Packag. Technol. 31 (2008) 11.
[45] S.K. Hsu, T.F. Morse, Kinetic theory of parallel plate heat transfer in a polyatomic gas, Phys. Fluids 15 (1972) 584–591.
[46] A.R. Peeketi, M. Moscardini, A. Vijayan, Y. Gan, M. Kamlah, R.K. Annabattula, Effective thermal conductivity of a compacted pebble bed in a stagnant gaseous environment: an analytical approach together with DEM, Fusion Eng. Des. 130 (2018) 80–88.
[47] ABAQUS Documentation, RI, USA, (2013).
[48] M. Gustavsson, E. Karawacki, S.E. Gustafsson, Thermal conductivity, thermal diffusivity, and specific heat of thin samples from transient measurements with hot disk sensors, Rev. Sci. Instrum. 65 (1994) 3856.
[49] Y. He, Rapid thermal conductivity measurement with a hot disk sensor, Thermochim. Acta 436 (2005) 122–129.
[50] S. Pupeschi, R. Knitter, M. Kamlah, Effective thermal conductivity of advanced ceramic breeder pebble beds, Fusion Eng. Des. 116 (2017) 73–80.
[51] A. Abou-Sena, A. Ying, M. Abdou, Effective thermal conductivity of lithium ceramic pebble beds for fusion blankets: a review, Fusion Sci. Technol. 47 (2005) 7.
[52] X.Z. An, R.Y. Yang, R.P. Zou, A.B. Yu, Effect of vibration condition and inter-particle frictions on the packing of uniform spheres, Powder Technol. 188 (2008) 102–109.
[53] W. Dai, J. Reimann, D. Hanaor, C. Ferrero, Y. Gan, Modes of wall induced granular crystallisation in vibrational packing, Granul. Matter 21 (2019) 26.
[54] J. Russo, H. Tanaka, The microscopic pathway to crystallization in supercooled liquids, Sci. Rep. 2 (2012) 505.
[55] C.H. Rycroft, G.S. Grest, J.W. Landry, M.Z. Bazant, Analysis of granular flow in a pebble-bed nuclear reactor, Phys. Rev. 74 (2006) 021306.
[56] B.R. Wang, J.T. Liu, S.T. Gu, Q.C. He, Numerical evaluation of the effective conductivities of composites with interfacial weak and strong discontinuities, Int. J. Therm. Sci. 93 (2015) 1–20.
[57] G. Rajoriya, C. Vijay, P.A. Ramakrishna, Thermal conductivity estimation of high solid loading particulate composites: a numerical approach, Int. J. Therm. Sci. 127 (2018) 252–265.
[58] P.-R. ten Wolde, M.J. Ruiz-Montero, D. Frenkel, Simulation of homogeneous crystal nucleation close to coexistence, Faraday Discuss 104 (0) (1996) 93–110.
[59] P.J. Steinhardt, D.R. Nelson, M. Ronchetti, Bond-orientational order in liquids and glasses, Phys. Rev. B 28 (2) (1983) 784–805.